

Influences of subseasonal to interannual oscillations on the SCS summer monsoon onset in 2018

Mong-Ming Lu, Chung-Hsiung Sui*, Ji-Ren Sun, and Po-Hsiung Lin

Department of Atmospheric Sciences, National Taiwan University, Taipei City, Taiwan

Article history:

Received 31 May 2019

Revised 20 February 2020

Accepted 25 February 2020

Keywords:

South China Sea summer monsoon, East Asian monsoon, Monsoon onset, ENSO, ISO, BSISO, MJO, Equatorial Rossby waves

Citation:

Lu, M.-M., C.-H. Sui, J.-R. Sun, and P.-H. Lin, 2020: Influences of subseasonal to interannual oscillations on the SCS summer monsoon onset in 2018. *Terr. Atmos. Ocean. Sci.*, 31, 197-209, doi: 10.3319/TAO.2020.02.25.01

ABSTRACT

The seasonal transition from December 2017 to May 2018 occurred during the final decaying stage of the La Niña phase following the 2015/16 El Niño. In this report we documented the anomalous cyclonic flow that persisted over the South China Sea (SCS) in winter and over the western North Pacific in spring was maintained by the anomalous heating in the equatorial Pacific and the extratropical influences that consist of weakened Aleutian low and subtropical wind-SST coupled air-sea fluxes over the NW Pacific. Persistent anomalous north-easterlies along with negative OLR and warm SST anomalies over the SCS in spring was found to be sustained by the cold and dry air advected from East Asia into the lower latitudes through the anomalous easterlies associated with the cyclonic flow to the south and anticyclonic flow to the north at 20 - 30°N. Besides the above interannual scale influences, heating over tropical Indian Ocean (IO) associated with two intra-seasonal oscillation (ISO) episodes in April and May caused strong easterly flow over eastern IO and Maritime Continent. The interannual and intra-seasonal influences together maintained an anticyclonic flow from SCS to Bay of Bengal in April and May, and delayed the SCS monsoon onset. A dry Equatorial Rossby wave that arrived at the SCS in late May further enhanced the delay and resulted in a late SCS monsoon onset in early June.

1. INTRODUCTION

The South China Sea (SCS) is part of the western Pacific marginal seas with Taiwan and Taiwan Strait as its northern limits and Singapore and the Strait of Malacca as the southern limits. The unique geographic location makes the SCS an interesting hotspot of research, in particular for understanding the relationship between East Asian monsoons and the air-sea coupled variation over the Pacific and Indian Oceans (IO). Several international field experiments conducted in the region currently are still ongoing such as Years of the Maritime Continent (YMC, <http://www.jamstec.go.jp/ymc/>), NASA Cloud and Aerosol Monsoonal Processes-Philippines Experiment (CAMP2Ex, <https://espo.nasa.gov/camp2ex/content/CAMP2Ex>), and the NOAA Climate Variability and Predictability (CVP) Program (<https://cpo.noaa.gov/Meet-the-Divisions/Earth-System-Science-and-Modeling/CVP>). Taiwan joined the international effort by conducting the SCS Two-Island Monsoon Experiment (SC-

STIMX) in corporation with the international YMC project to study convective and large-scale dynamic processes over the SCS and Maritime Continent (MC) region. A pilot study (December 2016) and two field campaigns during the Intensive Observation Periods (IOPs) (May to June 2018 and December 2018 to January 2019) were performed at Taiping Island and Dongsha Island within the extended observation period of 2017 - 2019 (Lin et al. 2016; Chen et al. 2020; Sui et al. 2020). The SCS summer monsoon (SCSSM) onset and Taiwan Mei-yu is a research focus for the first IOP, with a specific goal of improving the understanding and predictability of multi-scale convection over the region of study.

The large scale atmospheric circulation variability over the SCS-MC region involves the monsoon, intraseasonal oscillations, and convectively coupled waves. The SCSSM onset signifies a precursor of the establishment of the East Asian summer monsoon (EASM) (Wang et al. 2004; Chang et al. 2005). The onset process is characterized by the reversal of low-level zonal wind from easterlies to westerlies and a seasonal transition from the dry to wet regime over the central SCS from 5 to 15°N and 110 to 120°E, which is

* Corresponding author
E-mail: sui@as.ntu.edu.tw

usually associated with a retreat of the westward extension of the western North Pacific subtropical high (WPSH) from the SCS to the Philippine Sea (Mao et al. 2004). Mao et al. (2004) documented the seasonal evolution of the WPSH of which the ridge position over the SCS is defined as the westerly-easterly boundary surface, a line that separates westerlies to the north and easterlies to the south. They demonstrated that the seasonal shift of monsoonal flows is associated with the change in pressure distribution over the tropics, subtropics and midlatitude regions. The migration of tropical convection and the seasonal transition axis defined by the vertical characteristics of the westerly-easterly boundary surface indicate that climatologically the establishment of the Asian summer monsoon consists of at least three stages, first over the Bay of Bengal and the Indochina Peninsula, then the SCS and finally South Asia. The interannual (e.g., Zhou and Chan 2007; Luo et al. 2016) and interdecadal (e.g., Kajikawa and Wang 2012) variations of the SCS summer monsoon onset timing have been studied. Strong modulation by tropical intraseasonal oscillations was also documented (e.g., Kajikawa and Yasunari 2005; Tong et al. 2009).

The establishment of the SCSSM tends to be delayed after an El Niño winter due to the enhanced WPSH induced by the anomalous subsidence associated with the El Niño warm SST over the central and eastern equatorial Pacific. In contrast, the SCSSM after the La Niña winter tends to be established earlier than normal due to a persistent anomalous Philippine Sea cyclonic circulation from winter to the subsequent summer (see Liu and Zhu 2019, and the references therein). In addition to the remote ENSO forcing, the thermodynamic feedback between the anomalous cyclonic circulation and the underlying compensating warm SST anomalies over the western Pacific warm pool can sustain the anomalous cyclonic circulation for many months until the mean flow completely changes from the northeasterly trade winds in the winter regime to the westerly monsoonal flow in the summer regime (Wang et al. 2000, 2003).

On the other hand, the atmosphere over the SCS is known to process strong sub-seasonal variations mainly on the quasi bi-weekly (QBW, 12 - 25 days) and intra-seasonal (30 - 60 days) time scales (Zhou and Chan 2005, 2007; Hung and Hsu 2008; Wang et al. 2009; Chen and Sui 2010; Hung and Sui 2018). The QBW mode over the SCS has distinctly different propagation characteristics from the intra-seasonal oscillations (ISO, 30 - 60 days), which is also called boreal summer intraseasonal oscillation (BSISO) for the extended boreal summer (May to October) season. In their composite analysis study Kemball-Cook and Wang (2001) found significant differences in BSISO between the early (May to June) and late (July to October) summer months. They pointed out that Rossby waves play a critical role in the structure. Regardless early or late summer, eastward propagation convective anomalies are observed over the IO during the initiation stages of the ISO, followed by poleward-moving

Rossby waves (Jiang et al. 2004; Drbohlav and Wang 2005; Weng and Yu 2010; DeMott et al. 2013). After the initiation stages, the eastward propagating convective anomalies can move from the IO through the MC to western Pacific. The eastward propagating anomalies and the poleward moving Rossby waves form a northwest-southeast elongated convective anomalies that is distinctly different from the structure of the eastward propagating Madden-Julian Oscillation (MJO) (Madden and Julian 1971). The off-equatorial westward-propagating QBW mode is perceived as a moist equatorial Rossby (ER) wave modified by the basic state or a mixed Rossby-Gravity (MRG) wave (see Wang et al. 2009 and references therein).

The SCSTIMX first IOP (May to June 2018) was characterized as a monsoon transition season following a La Niña winter. Although the cyclonic anomalies sustained by the anomalous warm SST and air-sea interaction over the Philippine Sea and western Pacific was observed during the transition season, the SCSSM was not established until pentad 31 (31 May to 4 June) which was half-month later than the normal onset time in pentad 28 (16 - 20 May). The dramatic difference between 2018 and the other SCSSM onset evolution is clearly illustrated using the low-level zonal wind index (Uscs) calculated as the mean u-component of the wind field at 850 hPa averaged over the central SCS from 5 to 15°N and 110 to 120°E. Wang et al. (2004) documented that Uscs is a good index to represent the timing of the broad-scale summer monsoon seasonal transition over East Asia and the western North Pacific region (0 - 40°N, 100 - 140°E). Figure 1 shows that for the 13 years (1984, 1985, 1989, 1996, 1999, 2000, 2001, 2006, 2008, 2009, 2011, 2012, and 2017) of the April-June period that followed the La Niña winter the seasonal transition of Uscs from the easterlies to the westerlies, on average, is earlier than the climatological mean evolution. Here the La Niña winter is identified based on the cold DJF of “Historical El Niño/La Niña episodes (1950 - present)” published at the NOAA/Climate Prediction Center ENSO webpage at https://origin.cpc.ncep.noaa.gov/products/analysis_monitoring/ensostuff/ONI_v5.php. It is evident in Fig. 1 that all years following La Niña winters, indicated by the blue line with the standard deviate bars, show the transition from negative Uscs to positive occurred before 26 May, while the 2018 transition occurred on 1 June.

The late onset of the 2018 SCSSM was documented in Liu and Zhu (2019). Liu and Zhu (2019) attributed the late onset to the formation of a persistent anomalous barotropic anticyclone over Northeast Asia from mid- to late-May. The anomalous anticyclone reduced upper level divergence over the SCS, weakened the South Asian High and weakened the vertical easterly shear, therefore, helped to inhibit the development of convection over northern SCS.

In this paper we will discuss the late onset from a different perspective from Liu and Zhu (2019) by showing

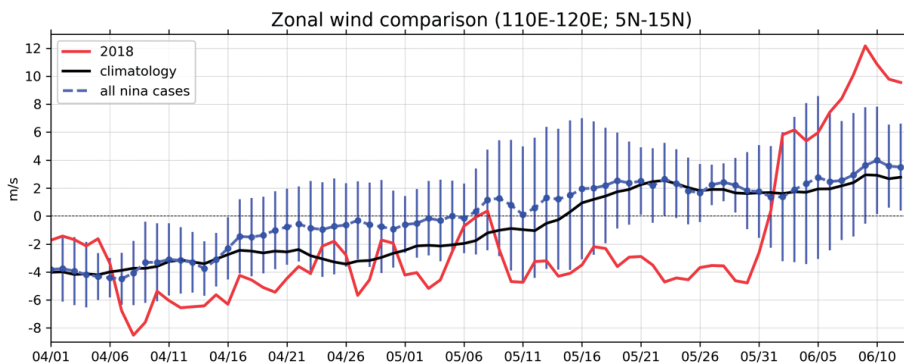


Fig. 1. Domain-averaged zonal wind over the SCS for the year of 2018 (red line), climatology (black line) and the 13-year average during La Niña decaying year (blue line) with 1 standard deviation (vertical blue line). Climatology is defined as the daily-averaged value during 1980 - 2017, and the La Niña year is defined as 1984, 1985, 1989, 1996, 1999, 2000, 2001, 2006, 2008, 2009, 2011, 2012, and 2017.

that the influence of BSISO and ER waves is the key factor. The data and the ISO and tropical wave identification methods are described in section 2. The climate background of the SCSTIMX observation period from 2017 to 2018 is presented in section 3. Section 4 discusses the influence of the tropical Pacific and IO on SCSSM. Section 5 discusses the influence of tropical intraseasonal oscillations on 2018 SCSSM onset. The combined influence of La Niña and intraseasonal oscillations on the SCSSM onset is presented in section 6. Section 7 is the conclusions and discussions.

2. DATA AND METHODOLOGY

In this section, we describe the primary data sets and analysis methods. Additional data or analysis procedure used in some specific figures will be described in corresponding discussions. The analysis is based on the European Center for Medium-Range Weather Forecasts (ECMWF) interim reanalysis (Dee et al. 2011) with a temporal resolution of 6-hr and at $0.75^\circ \times 0.75^\circ$ horizontal resolution at 60 vertical levels from the surface up to 0.1 hPa. The variables include the mean sea level pressure (SLP), horizontal and vertical velocity (u , v , and w), specific humidity (q), horizontal vorticity and derived velocity potential (ψ) and stream function (sf) from u and v . We also analyzed two sets of SST data: the NOAA Extended Reconstructed Sea Surface Temperature (ERSST v5; Huang et al. 2017) of monthly and $2^\circ \times 2^\circ$ horizontal resolution, and the Optimum Interpolation Sea Surface Temperature (OISST) of daily and $0.25^\circ \times 0.25^\circ$ resolution. For the proxy of convection activities, we used National Oceanic and Atmospheric Administration (NOAA) Climate Data Record (CDR) of daily outgoing long-wave radiation (OLR) version 1.2 (Liebmann and Smith 1996; Lee and NOAA CDR Program 2011) with $1^\circ \times 1^\circ$ resolution estimated from High-Resolution Infrared Radiation Sounder (HIRS) radiance observation with a two-day lag. For precipitation we use Global Precipitation Climatology Project (GPCP) Version 2.3 monthly precipita-

tion data set at $2.5^\circ \times 2.5^\circ$ spatial resolution (Huffman et al. 1997; Adler et al. 2018).

The monthly climatological fields of all variables are defined by the mean fields of each calendar month between January 1980 and December 2017. The monthly anomalies are defined by deviations from the corresponding monthly climatological fields. The daily climatological fields are defined as the summation of the first-three harmonics of daily annual cycle. Daily anomalies are the difference between original daily data and the daily climatology.

The SCSSM onset index is defined as the 850-hPa zonal wind averaged in the area of $110 - 120^\circ\text{E}$ and $5 - 15^\circ\text{N}$ (Wang et al. 2004). The circulation index such as the 850-hPa vorticity is averaged 5 degrees of latitude north to the Usus index as $10 - 20^\circ\text{N}$. The La Niña cases are selected when the Ocean Niño Index (ONI), provided by NOAA's Climate Prediction Center (<https://www.cpc.ncep.noaa.gov/>), is below 0.5°C . The anomalies are calculated based on centered 30-year base periods updated every 5 years.

Variables of convection-coupled waves are defined based on the space-time filtering procedures by Wheeler and Hendon (2004). The major variables including OLR and u at 850 and 200 hPa are filtered to resolve the MJO, Kelvin wave (KW) and ER. The corresponding ranges of wave number and frequency for the MJO and the two wave modes are presented in Table 1. The detailed procedure is described in Chen et al. (2019) and Tsai et al. (2020). The MJO during the boreal summer season (BSISO) often bifurcates to northward- and eastward-moving components over the western IO and results in a northwest-southeast elongated convective anomalies after passing the center IO with a structure distinctly different from the MJO. Because in the present study the focus is on ISO, we will not rigorously separate the eastward moving ISO to BSISO or MJO, instead will call the subtropical ISO as BSISO and the equatorial ISO as MJO.

The winter, spring and summer in this work are defined following the general usage, namely DJF, MAM, and JJA.

The 2018 winter means the three-month period of December 2017 and January to February 2018. The 2018 spring means the three-month period of March-April-May in 2018.

3. CLIMATE BACKGROUND OF THE SCSTIMX 2017 - 2018

3.1 ENSO Features from December 2016 to June 2018

The spring to early summer season of 2018 was in the final stage of the La Niña phase following the 2015/16 El Niño as shown by longitude-time (Hovmöller) diagram of anomalous SST, OLR, and wind at 850 hPa along the equator between 5°S and 5°N during the period from 2016/12 to 2018/06 (Fig. 2). Here the anomaly is defined by the deviation from long-term (1980 - 2017) mean and the first-three harmonic computed from the data of 1980 - 2017. A 11-day moving-average is used on all variables to filter out high frequency wave. Figure 2a shows cold SST anomaly (SSTA) in central and eastern Pacific emerged in the late summer of 2017 became intensified during winter of 2017/18 and substantially decayed after spring 2018 and turned to positive in May and June. Figure 2b shows a pattern of enhanced equatorial convection over western Pacific and eastern IO from the winter of 2016/17 until spring 2018. Associated with the enhanced convection, to its east is mostly the easterly (negative) anomalies. The westerly (positive) anomalies occurred concurrently with the negative anomalies of the OLR. It shows that deep convection tends to occur when the low-level wind anomalies are positive.

The seasonal mean anomalies of SST, SLP, 850-hPa winds and stream function for December to February and March to May 2018 are presented in Fig. 3. The anomalies are computed by removing the annual cycle based on the 30-year average of the 3-month running mean from 1981 to 2010. Note that in Fig. 3 we used the current climatological standard normal period 1981 - 2010 (WMO 2017) for calculating the ENSO associated seasonal features, whereas for the sub-seasonal features such as monsoon onset and planetary-scale waves and monthly anomalies we use the data from 1980 to 2017 to represent the background climate. The La Niña winter (Figs. 3a and c) was characterized by strong eastern Pacific cold tongue, suppressed convection over the central equatorial Pacific, and enhanced Intertropical Convergence Zone (ITCZ) on both sides of the equator along

with strong trade wind and an anomalous cyclonic circulation over the SCS. The tropical features described above are maintained by equatorial climate dynamics (e.g., Wang et al. 2000). In addition, the La Niña winter also exhibits notable extratropical features of weakened Aleutian low/westerly jet (Fig. 3c), warm SST in north Pacific similar to the Pacific Meridional Mode (PMM) (Chiang and Vimont 2004). From the winter to spring, the overall La Niña features generally remained but the warm SST and wind associated with the PMM and the anomalous anticyclonic circulation over north Pacific persisted and moved southwestward to western Pacific near 140°E where an anomalous cyclonic circulation and enhanced convection appeared east of Philippine Sea. This is attributed to the seasonal footprinting mechanism in the Pacific (Vimont et al. 2003; Chang et al. 2007) and the basin-scale ocean-atmosphere coupled mode also known as the Victoria mode (VM) (Tseng et al. 2017a, b). The VM is the second dominant mode (EOF2) of springtime North Pacific SST anomalies poleward of 20°N. It has a significant impact on the Pacific ITCZ precipitation during the following summer and ENSO evolution during the following winter, and is closely linked to the intensity of the SCS summer monsoon (Ding et al. 2018).

The decaying cold SST anomaly in the winter of DJF 2018 was coupled with a well-organized ISO with strong westerly and negative OLR anomalies propagating from IO to central Pacific near 150°W during the winter. In the following spring 2018, two ISOs were respectively observed in April and May associated with active convection confined over eastern and central IO.

3.2 Features of the Spring Season After La Niña Winter in 2018

The monthly mean anomalous fields of SST, OLR, and 850-hPa wind for March, April, and May 2018 (Figs. 4a - f) show a weakening tendency of the negative SST anomaly over the equatorial and South Pacific and South IO from March to May. The weakening tendency was associated with the weakening La Niña. However, over the western North Pacific, from Taiwan to a reference point such as (30°N, 180°E), a southwest-northeast elongated warm SST anomaly persistently developed from March to May. This SST anomaly resembles the VM pattern over the mid-latitude

Table 1. The range of zonal wavenumber, period (day) and equivalent depth (m) chosen for filtering MJO, Kelvin wave, and equatorial Rossby wave. The wavenumber-frequency ranges for MJO, Kelvin wave, ER wave are based on Wheeler and Kiladis (1999).

| | Zonal wave number | Period (day) | Equivalent depth (m) |
|------------------------|-------------------|--------------|----------------------|
| MJO | 1 to 5 | 30 to 90 | - |
| Kelvin wave | -10 to -1 | 9.7 to 48 | 8 to 90 |
| Equatorial Rossby Wave | 1 to 14 | 2.5 to 30 | 8 to 90 |

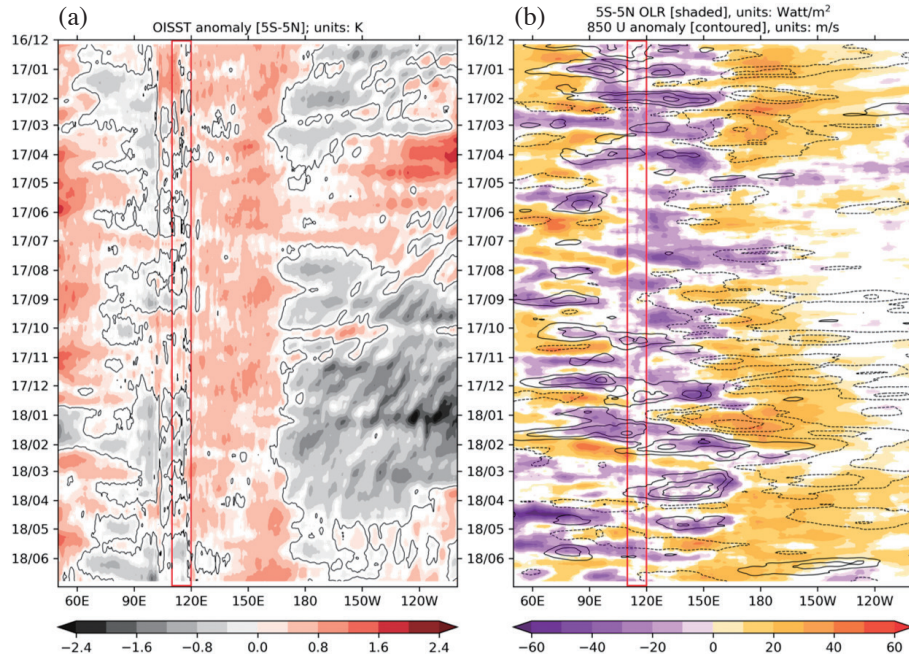


Fig. 2. Hovmöller for interannual-scale SST (a), OLR and zonal wind (b) anomaly on the equator. Anomaly is defined by the value in 2018 subtracting long-term average and the first-three harmonic during 1980 - 2017 and a 11-day moving-average is used on all variables to filter high frequency wave. Black line in (a) shows the 0-value line for SST anomaly. Solid (dashed) line in (b) displays westerly (easterly) with the interval of 2 m s^{-1} , and the 0-value line is omitted.

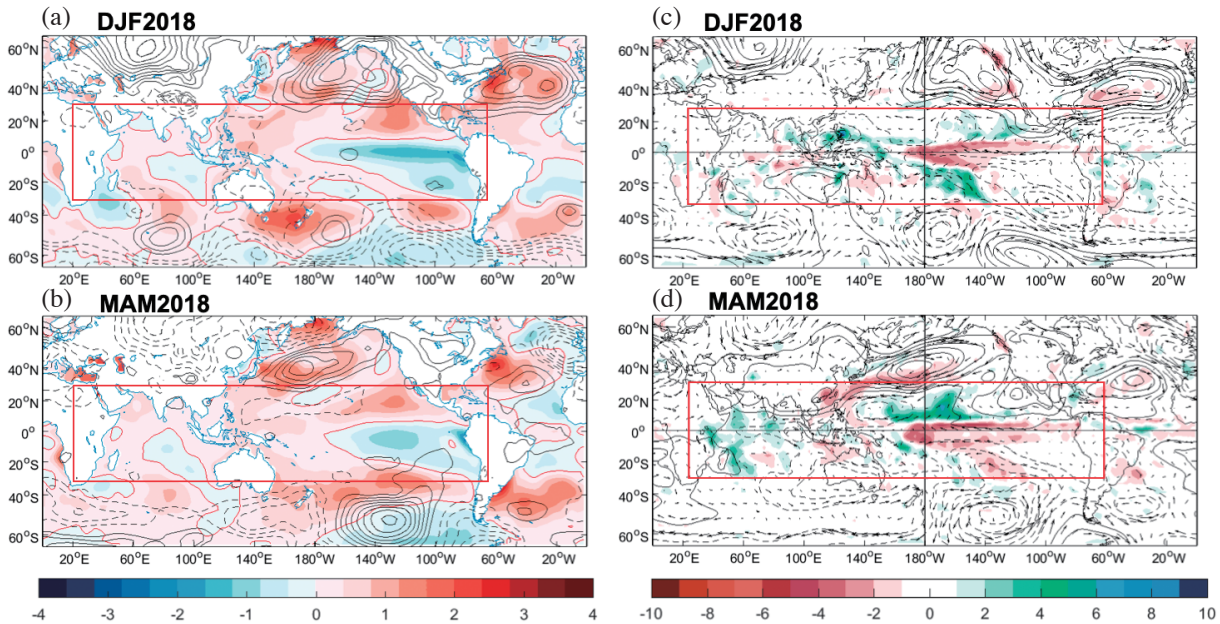


Fig. 3. The 2018 anomalies of the SST, SLP, precipitation, 850-hPa winds. The winter season DJF is shown in (a) and (c) and the spring season MAM is shown in (b) and (d). (a) - (b) are the SST (shadings, unit: $^{\circ}\text{C}$) and SLP (contour interval: 1 hPa) anomalies, (c) - (d) are the precipitation (shadings, unit: mm day^{-1}), 850-hPa stream function (contour interval: $10^6 \text{ m}^2 \text{ s}^{-1}$) and wind vector anomalies. The anomalies in (c) - (d) are computed as the difference between the raw data and the 30-year climatology.

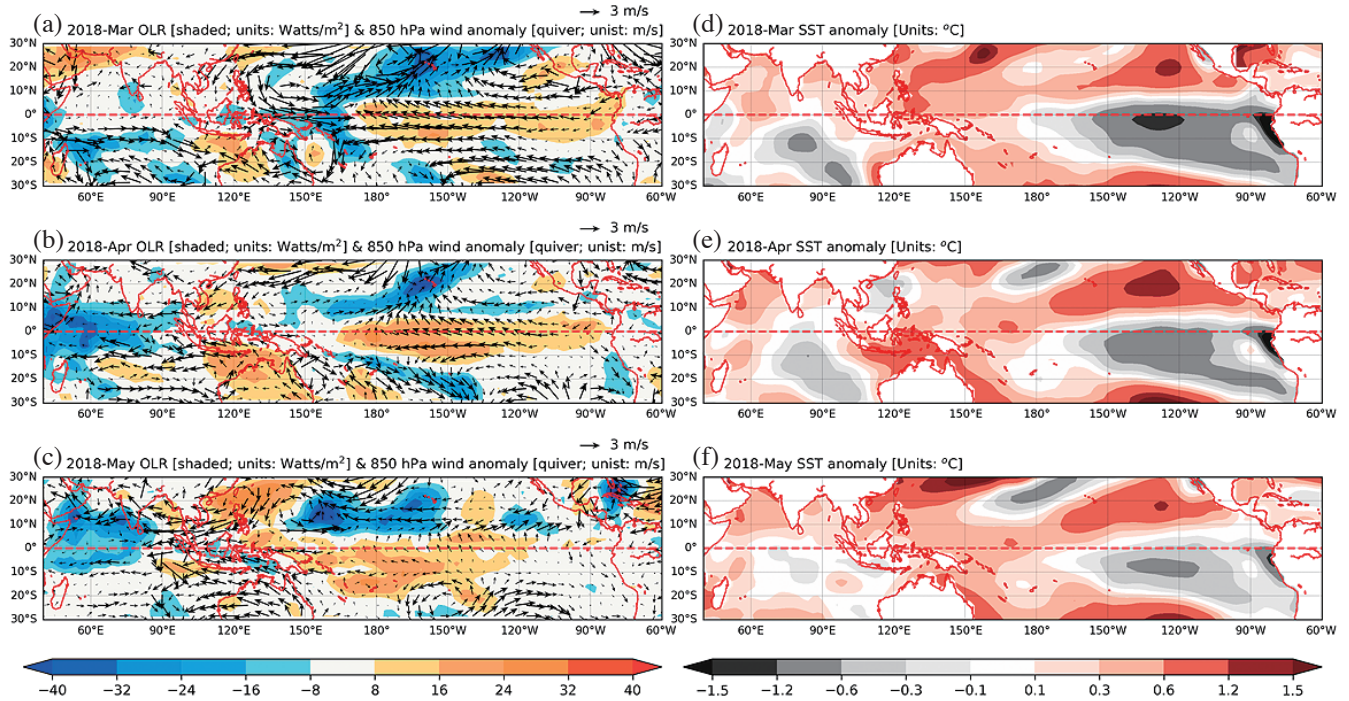


Fig. 4. Monthly anomaly OLR and 850-hPa horizontal wind [shaded and quiver in (a), (b), (c)] and SST [(d), (e), (f)] anomaly from March to May [(a) to (c) and (d) to (f)] are demonstrated. Anomaly is defined as the difference between 2018 and the climatology which is the monthly average from 1980 to 2017.

North Pacific region, but with enhanced warm SST anomaly extended to the western boundary ocean near Taiwan. The southwestward SST warm anomaly extension can be a response to the positive SLP anomaly in Fig. 3b that creates a favorable condition for the west boundary ocean surface to absorb more solar heating. Persistent warm SST anomaly is also observed over North IO in particular the Arabian Sea, Bay of Bengal and the SCS. During these three months the SSTs over the western Pacific tropical warm pool (0 - 15°N, 120 - 150°E) were warmer than climatology.

The large-scale convection and circulation represented by OLR and 850-hPa wind anomalies in Fig. 4 illustrate some important features associated with the weakened La Niña. The easterly anomaly over the equatorial central Pacific (160°E - 160°W) rapidly weakened from March to May. Over North Pacific we see clear negative OLR anomaly and the southwest-northeast oriented anomalous cyclonic circulation suggesting stronger tropical and subtropical convective weather activity in March (Figs. 4a, d). Note that the anomalous cyclonic circulation is associated with the subtropical warm SST anomaly extended from the subtropical eastern Pacific, between Hawaii and Mexico, southwestward to the western Pacific warm pool (Fig. 4d). The subtropical (20 - 30°N) warm SST over western North Pacific (Fig. 4d) is associated with the extratropical easterly anomalies over the western Pacific (Fig. 4a) reflecting the weaker than normal Aleutian Low. The off-equatorial westerly anomalies along 5°N in May can enhance the central

Pacific ITCZ (Fig. 3d) and the associated cyclonic circulation as a Gill type response with the Rossby wave response to the west of the diabatic heating associated with the convective center and Kelvin wave to the east of the heating center. The cyclonic anomaly is in favor of exciting an anticyclonic response to its west which can induce the eastward propagation of the SCS anticyclone anomaly and the associated downwelling Kelvin wave, and eventually terminate the La Niña and trigger an El Niño similar to the VM mechanism proposed in Ding et al. (2015a, b). Figure 4b shows the cyclonic anomaly over SCS gradually moved to the western Pacific near 160°E from March to May. Over the IO, active convection (or negative OLR anomalies) appeared in western-central areas around equatorial zone in April and more to the north near 10°N in May. The negative OLR is associate with warm SST anomalies (Fig. 4f). Anomalous warm SST and enhanced convection over IO maintain the subtropical easterlies from the SCS through the Bay of Bengal to the Arabian Sea.

4. THE INFLUENCES OF THE TROPICAL PACIFIC AND INDIAN OCEAN ON SCS

In order to understand the large-scale environment influence on the SCSSM onset, we examined the time and longitude cross section of anomalous vorticity (10 - 20°N average) and zonal wind (5 - 15°N average) at 850 hPa (Fig. 5). The two variables are smoothed by a 3-day running

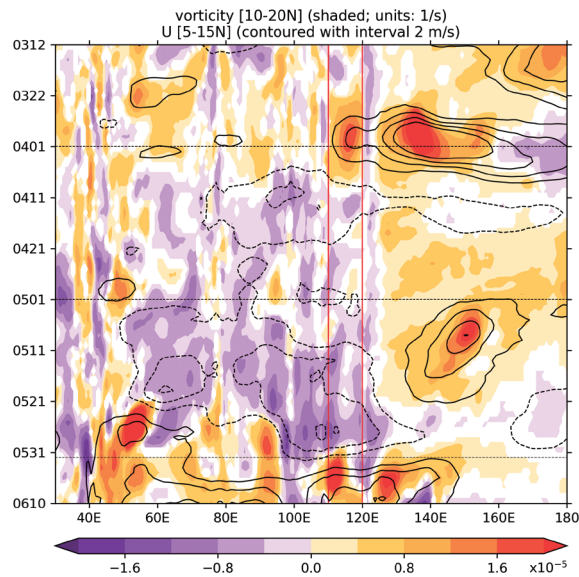


Fig. 5. Meridional-averaged 850 hPa vorticity anomaly between 10 - 20°N (shaded) and zonal wind anomaly between 5 - 15°N (contour) are displayed. Shaded in red (purple) means (anti)cyclonic circulation and solid (dashed) contour means westerly (easterly) with the interval of 2 m s^{-1} from -8 to 8 m s^{-1} . The 0-value contour for zonal wind was omitted. A 3-day running-average smooth is used on both vorticity and zonal wind.

average. To the east of the Philippines (125°E) the vorticity is in general positive with two maxima during the periods of from late March to early April and from mid-April to early May, with the centers at 135°E and 150°E , respectively. The positive vorticity in Fig. 5 that reflects cyclonic circulation over the Philippine Sea and western Pacific (Fig. 4) is an air-sea coupled response to the La Niña forcing (Wang et al. 2000). To the west of the Philippines the vorticity from the SCS to eastern IO (90°E) is generally negative during April and May. The negative vorticity in Fig. 5 is consistent with the anticyclonic circulation observed in Fig. 4b over the northern SCS, Southeast Asia and the Bay of Bengal. Two episodes of persistent easterlies appeared over IO and SCS. The first easterly episode over SCS ($110 - 120^\circ\text{E}$) in 10 - 20 April occurred after the enhancement of the easterlies over the Bay of Bengal ($90 - 100^\circ\text{E}$). This is a response to the MJO heating over eastern and central IO in April. The second easterly episode over SCS in 12 - 30 May reflects the effect of eastward propagating easterly anomalies associated with the anticyclonic vorticity from 50 to 90°E over the Arabian Sea, India and the western Bay of Bengal. This is a response of the propagating BSISO heating over Indian Ocean in May. In fact, the fluctuations of the 850-hPa vorticity and u anomalies over the SCS indicate that the delayed SCSSM onset was associated with decaying La Niña-forced cyclonic circulation and ISO-induced suppression that were originated from the Pacific and IO, respectively.

5. ROLES OF TROPICAL INTRASEASONAL OSCILLATIONS

Both 30-60-day and 10-20-day oscillations were active in April and May 2018 as shown by the Hovmöller diagram of OLR anomalies and the filtered OLR at the MJO, ER, and KW bands averaged within two different latitudinal bands of $5^\circ\text{S} - 5^\circ\text{N}$ and $5 - 15^\circ\text{N}$ in Figs. 6a - b. The figure shows two eastward-moving bands of negative OLR anomalies over the equator from western IO to western Pacific (near 160°E) that correspond well with the filtered signal of the MJO (or 30-60-day oscillation) in April and May, respectively. The evolution of the two 30-60-day oscillations are also shown by the pentad mean OLR anomalies and velocity potential at 200 hPa in Fig. 7. Figures 6 and 7 show that the 30-60-day oscillation in April evolved from the growing stage during the half month and weakened rapidly afterward. Its convection is mostly confined in the western and central tropical IO that influenced SCS through its overturning circulation (Fig. 5). Following the convective phase of the MJO in April, a suppressed phase of the MJO was observed to move from western Indian Ocean (~ 28 April) to SCS (~ 13 May) and Philippine Sea (~ 18 May). Then another 30-60-day oscillation developed over western IO from near 10 May and moved both eastward and northward, resulting in a northwest-southeast oriented band of convection in the rest of May. SCS was in the suppressed phase of the 30-60-day oscillation in the pentad around 13 - 18 May.

Besides the 30-60-day oscillations, 10-20-day oscillations also known as ER waves were also active during April and May. The Hovmöller diagram of space-time filtered OLR within the ER frequency band averaged between $5 - 15^\circ\text{N}$ (Fig. 6b) shows how the waves evolve with time and interact with each other. Most ER waves during the two

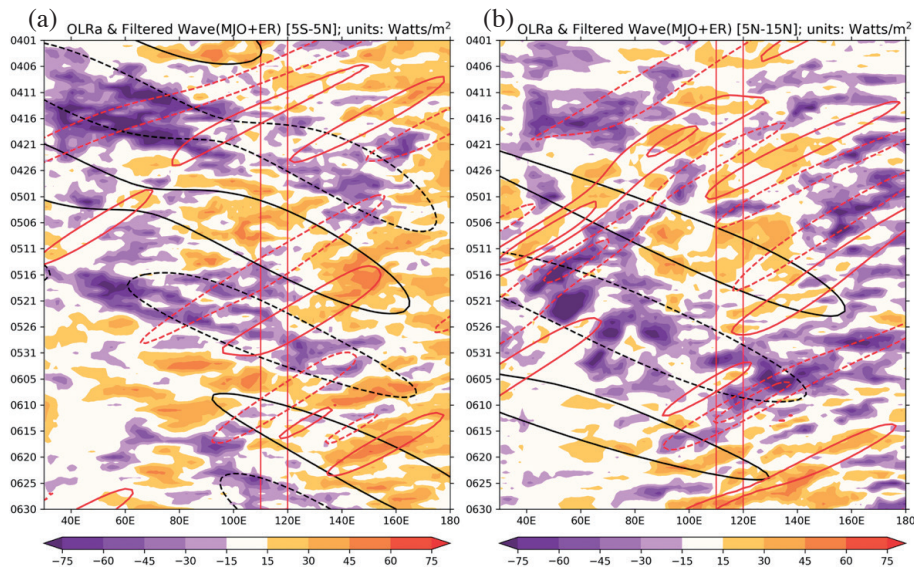


Fig. 6. Hovmöller diagrams for OLR anomaly on the equator (a) and north of the equator (b) were shown. The OLR anomaly was applied a 11-day running-average. Also shown in both figures is the ISO wave (black contour) and ER wave (red contour) calculated from the space-time filter. Solid (dashed) line means positive (negative) anomalous OLR with the interval of 10 Watt m⁻². 0-value contour is omitted.

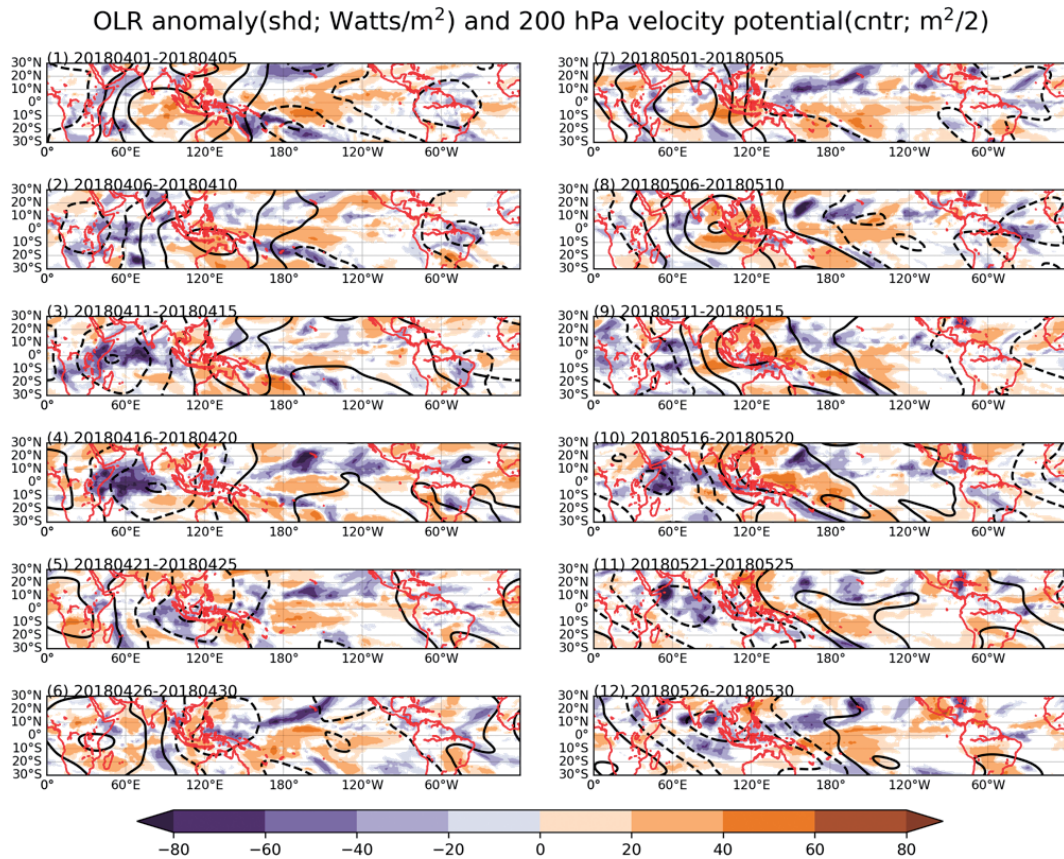


Fig. 7. Pentad-averaged maps for OLR anomaly (shaded) and 200 hPa velocity potential anomaly (contour) from April to May were demonstrated. Solid (dashed) contour means positive (negative) anomalous velocity potential with the interval of 2×10^6 (m² s⁻¹).

months originated in western Pacific and move westward to SCS. A dry pulse of ER wave moved into SCS in late May that appears to delay the monsoon onset for a few days as will be discussed in section 6. The spatial pattern of the large-scale waves can be clearly seen in the April to May pentad-averaged maps for OLR anomaly and 200-hPa vp anomaly presented in Fig. 7. The negative vp anomalies and the negative OLR anomalies that reflect tropical deep convection show good coherent relationship. OLR anomalies suggest that deep convection was active in April and May except during the two pentads from late April to early May. Prior to the suppression of IO deep convection the positive 200-hPa vp anomalies appeared over the eastern Atlantic and slowly moved through Africa into the IO. The deep convection became active again when the positive 200-hPa vp anomalies continuously moved eastward to the eastern IO and Indonesia MC. In late May (the bottom one on Fig. 7 right column) over the SCS-MC region we see a dipole pattern of the OLR with negative anomalies over the Indonesia MC and positive anomalies over the SCS. The negative anomalies over the Indonesia MC show good relationship with the negative 200-hPa vp. However, the positive anomalies over the SCS do not show good relationship with the 200-hPa vp anomalies. This evidence favors the possibility that the dry anomalies occurred during the normally active SCSSM pentad was not directly related to the dry phase of MJO, which is represented by the most pronounced eastward moving 200-hPa vp anomalies with a clear dipole structure, but suppressed by the dry ER wave.

The SCSSM onset was delayed by the suppressed west-

erlies over the SCS (Fig. 1). The longitude and latitude vertical cross sections of wind and moisture can help us to see how the 30-60-day and 10-20-day oscillation suppressed the development of the onset westerlies over the SCS. Figure 8a shows strong easterlies occupied the boundary layer lower than 700 hPa over the SCS during the 27th pentad (11 - 15 May). The low-level easterlies cover a wide longitudinal range from 60 to 120°E, which is consistent with the monthly mean easterly anomalies in May (Fig. 4) and wide-scale anticyclonic vorticity anomaly in Fig. 5. The strong upward motion over the IO is associated with the convective phase of the 10-20-day ER wave shown in Fig. 6. The passage of the ER wave through the Bay of Bengal (80°E) triggered two centers of the development of active convection, one around the southern tip of India and another over western Indian Ocean to the west of India Peninsula (70°E). These two convective centers are clearly depicted in Fig. 8a. The low-level easterlies suggest strong influence of the powerful convective circulation to the west of India that later evolve to the convective phase of the MJO or ISO or 30-60-day wave in Figs. 6 and 7. The downward motion over the SCS region (110 - 120°E, 10 - 20°N) in Figs. 8a - b suggest that the subsidence was more closely associated with the circulation in the east-west direction (Fig. 8a) than the north-south direction (Fig. 8b).

The prolonged low-level easterlies over the SCS can be clearly identified in the longitudinal vertical cross section in the 30th pentad (26 - 30 May) in Fig. 8c where we see the thick layer of the easterlies over the SCS and the Philippine Sea (110 - 150°E). The eastward propagating convective

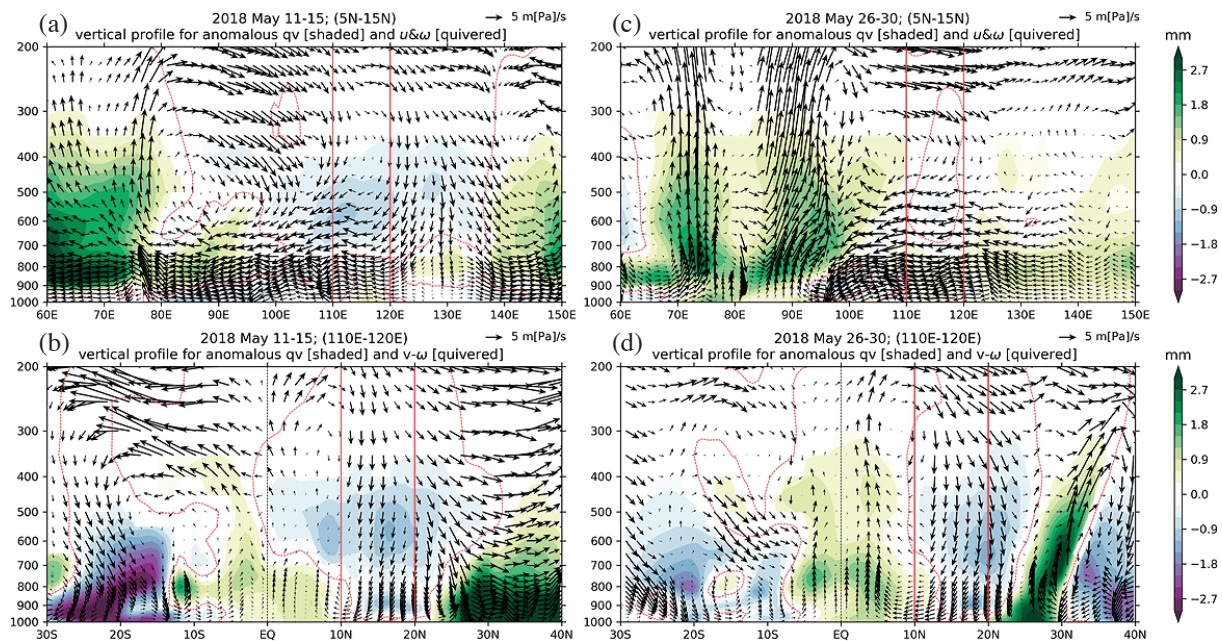


Fig. 8. Zonally cross sections (5 - 15°N) for u and w [quiver in (a), (c)] and meridionally cross sections (110 - 120°E) for v and w [quiver in (b), (d)] during specific pentad were demonstrated. (a) and (b) are the pentad during 11 - 15 May and (c) and (d) are the pentad during 26 - 30 May. Also shown in all figures are the anomalous specific humidity anomalies (shaded).

circulation of the 30-60-day oscillation (Figs. 6 and 7) is clearly shown in Figs. 8c - d. Different from the condition in mid-May, the downward motion over the SCS in late May is more associated with the meridional circulation that is associated with the convective center over the southern tip region of the SCS and maritime land regions around the Malay Peninsula and western Indonesia islands ($0 - 5^{\circ}\text{N}$). The near equator deep convection is part of the 30-60-day oscillation as illustrated in Fig. 7.

6. THE COMBINED INFLUENCES OF LA NIÑA AND INTRASEASONAL OSCILLATIONS ON THE SCSSM ONSET

To quantify the combined influence of interannual and intraseasonal oscillation on the SCS monsoon onset, we show in Fig. 9 the area-averaged anomalies of OLR and zonal wind within ($110 - 120^{\circ}\text{E}$, $5 - 15^{\circ}\text{N}$) spectrally separated into interannual, 30-60-day, 10-20-day, and the climatological annual cycle. The OLR values in Fig. 9 are anomalies from the time-mean of climatological annual cycle ($233.93 \text{ Watt m}^{-2}$). Note that the OLR in Fig. 9a is multiplied by a factor of -1 for the convenience of seeing the onset transition with Fig. 9b. The interannual anomalies are 60-day running averages of the total anomalies. Compared with the climatological onset day of zonal wind and OLR (near 16 and 21 May), the onset day of OLR and zonal wind of 2018 is about 2 pentads late near 31 May and 3 June. The delay in zonal wind is related to both the interannual and interseasonal (30-60-day and 10-20-day) oscillations. The delay in OLR is first related to the suppressed effect

by 30-60-day around 20 May and further suppressed by a 10-20-day oscillation in the remaining days of May until the combined 30-60-day and seasonal cycle to overcome the suppression of 10-20-day oscillation in early June.

7. CONCLUSIONS AND DISCUSSIONS

This study shows the analysis of large-scale background of the boreal winter and spring prior to the summer monsoon onset over SCS in 2018. This is the period the field campaign of the SCSTIMX was performed (Sui et al. 2020). From December 2017 to June 2018, SCS-MC and the surrounding IO and tropical Pacific Ocean were influenced by a decaying La Niña. The intraseasonal oscillations in April and May 2018 was quite pronounced. The La Niña oscillation in the winter and spring exhibits typical tropical features of strong east-west SST gradient and associated convective heating contrast, strong cyclonic circulation in lower troposphere residing over SCS in DJF and west Pacific in MAM 2018. The locations and seasonal evolution of the anomalous cyclonic circulation is related to weakened Aleutian low/westerly jet and a persistent northeast-southwest oriented SST anomalies over subtropical Pacific, suggesting strong tropical-extratropical interactions. The tropical SSTA/convection and subtropical circulation are shown to contribute to a persistent low-tropospheric anti-cyclonic flow from SCS to Bay of Bengal from April to May.

The broad scale anti-cyclonic circulation is shown to be maintained also by heating over IO associated with two 30-60-day oscillations occurred in April and May, respectively. The tropical heating caused persistent easterly winds

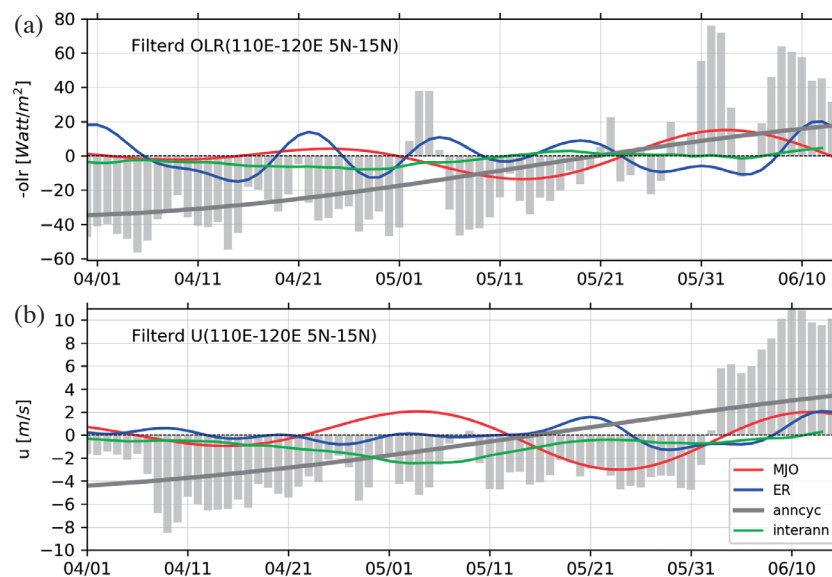


Fig. 9. Domain-averaged OLR (a) and zonal wind (b) over SCS region is demonstrated here. In both figures, the grey bar means the time-series in 2018, and the red and blue line indicate the band for MJO and ER wave separately. The grey line shows the annual cycle calculated from the summation of long-term average and the first-3 harmonic. The green line indicates the interannual component obtained from the 60-day running-average daily anomaly. In (a), the long-term averaged OLR ($233.93 \text{ Watt m}^{-2}$) is subtracted from the annual cycle component (grey line).

that is the southern portion of the anti-cyclonic circulation. The 30-60-day oscillation in May exhibits typical BSISO features of notable northward propagation in addition to eastward propagation. The BSISO and the interannual oscillation combined caused a delay of the SCS monsoon onset that is further delayed by a pronounced 10-20-day oscillation, the ER wave. The 10-20-day oscillation brought suppressed convection and easterly wind to SCS in late May. The 2018 case is unique compared with the ISO influence on the SCS summer monsoon onset documented in Wang et al. (2018) based on the 1980 - 2013 data. They found the late onset is usually delayed by the wet phase of southern Indian summer monsoon ISO, while in the 2018 case it was delayed by the wet phase over the equatorial Indonesia MC. More studies are needed to explore how ISO can influence the SCS summer monsoon.

The large-scale circulation and associated interannual oscillations in SST and convection suggest that the anomalous circulation over SCS and NW Pacific is influenced by both tropical and extratropical air-sea interaction. Our ongoing study suggests that extratropical influence is particularly strong in some prolonged ENSO events like 1986/87 and 2015/16 events. This raises some intriguing questions like how PMM and subtropical anomalous anticyclonic (cyclonic) circulation over the northwest Pacific and the SCS accompanied with El Niño (La Niña) add to ENSO diversity? What are the major modes of anomalous circulation over the Indo-Pacific region, in particular, the SCS and the Philippine Sea? Do they also exist in non-ENSO years? It also remains to be further explored about the maintenance mechanism of the persistent anomalous patterns during different seasons where different feedback and heating processes are involved if the prevailing winds are northeast or southwest monsoonal flow over the South China Sea.

Acknowledgements This study is supported by the Ministry of Science and Technology, Taiwan, Grant MOST 108-2111-M-002-009, MOST 105-2119-M-002-025, and MOST 106-2119-M-002-003-MY2.

REFERENCES

- Adler, R., M. Sapiano, G. Huffman, J.-J. Wang, G. Gu, D. Bolvin, L. Chiu, U. Schneider, A. Becker, E. Nelkin, P. Xie, R. Ferraro, and D.-B. Shin, 2018: The Global Precipitation Climatology Project (GPCP) Monthly Analysis (New Version 2.3) and a Review of 2017 Global Precipitation. *Atmosphere*, **9**, 138, doi: 10.3390/atmos9040138. [[Link](#)]
- Chang, C.-P., Z. Wang, J. McBride, and C.-H. Liu, 2005: Annual cycle of Southeast Asia—Maritime Continent rainfall and the asymmetric monsoon transition. *J. Clim.*, **18**, 287-301, doi: 10.1175/jcli-3257.1. [[Link](#)]
- Chang, P., L. Zhang, R. Saravanan, D. J. Vimont, J. C. H. Chiang, L. Ji, H. Seidel, and M. K. Tippett, 2007: Pacific meridional mode and El Niño-Southern Oscillation. *Geophys. Res. Lett.*, **34**, L16608, doi: 10.1029/2007GL030302. [[Link](#)]
- Chen, G. and C.-H. Sui, 2010: Characteristics and origin of quasi-biweekly oscillation over the western North Pacific during boreal summer. *J. Geophys. Res.*, **115**, D14113, doi: 10.1029/2009JD013389. [[Link](#)]
- Chen, J.-M., C.-H. Tsou, R. Wu, and C.-H. Sui, 2020: Introduction to the special issue on South China Sea Two-Island Monsoon Experiment (SCSTIMX): Observation, simulation, and projection. *Terr. Atmos. Ocean. Sci.*, **31**, 97-101, doi: 10.3319/TAO.2020.03.19.01. [[Link](#)]
- Chen, W.-T., S.-P. Hsu, Y.-H. Tsai, and C.-H. Sui, 2019: The Influences of Convectively Coupled Kelvin Waves on Multiscale Rainfall Variability over the South China Sea and Maritime Continent in December 2016. *J. Clim.*, **32**, 6977-6993, doi: 10.1175/jcli-d-18-0471.1. [[Link](#)]
- Chiang, J. C. H. and D. J. Vimont, 2004: Analogous Pacific and Atlantic meridional modes of tropical atmosphere-ocean variability. *J. Clim.*, **17**, 4143-4158, doi: 10.1175/jcli4953.1. [[Link](#)]
- Dee, D. P., S. M. Uppala, A. J. Simmons, P. Berrisford, P. Poli, S. Kobayashi, U. Andrae, M. A. Balmaseda, G. Balsamo, P. Bauer, P. Bechtold, A. C. M. Beljaars, L. van de Berg, J. Bidlot, N. Bormann, C. Delsol, R. Dragani, M. Fuentes, A. J. Geer, L. Haimberger, S. B. Healy, H. Hersbach, E. V. Hólm, L. Isaksen, P. Kållberg, M. Köhler, M. Matricardi, A. P. McNally, B. M. Monge-Sanz, J.-J. Morcrette, B.-K. Park, C. Peubey, P. de Rosnay, C. Tavolato, J.-N. Thépaut, and F. Vitart, 2011: The ERA-Interim reanalysis: Configuration and performance of the data assimilation system. *Q. J. R. Meteorol. Soc.*, **137**, 553-597, doi: 10.1002/qj.828. [[Link](#)]
- DeMott, C. A., C. Stan, and D. A. Randall, 2013: Northward Propagation Mechanisms of the Boreal Summer Intraseasonal Oscillation in the ERA-Interim and SP-CCSM. *J. Clim.*, **26**, 1973-1992, doi: 10.1175/JCLI-D-12-00191.1. [[Link](#)]
- Ding, R., J. Li, Y. Tseng, C. Sun, and Y. Guo, 2015a: The Victoria mode in the North Pacific linking extratropical sea level pressure variations to ENSO. *J. Geophys. Res.*, **120**, 27-45, doi: 10.1002/2014jd022221. [[Link](#)]
- Ding, R., J. Li, Y. Tseng, and C. Ruan, 2015b: Influence of the North Pacific Victoria mode on the Pacific ITCZ summer precipitation. *J. Geophys. Res.*, **120**, 964-979, doi: 10.1002/2014jd022364. [[Link](#)]
- Ding, R., J. Li, Y. Tseng, L. Li, C. Sun, and F. Xie, 2018: Influences of the North Pacific Victoria Mode on the South China Sea summer monsoon. *Atmosphere*, **9**, 229, doi: 10.3390/atmos9060229. [[Link](#)]

- Drbohlav, H.-K. L. and B. Wang, 2005: Mechanism of the northward-propagating intraseasonal oscillation: Insights from a zonally symmetric model. *J. Clim.*, **18**, 952-972, doi: 10.1175/jcli3306.1. [[Link](#)]
- Huang, B., P. W. Thorne, V. F. Banzon, T. Boyer, G. Chepurin, J. H. Lawrimore, M. J. Menne, T. M. Smith, R. S. Vose, and H.-M. Zhang, 2017: Extended Reconstructed Sea Surface Temperature, Version 5 (ERSSTv5): Upgrades, Validations, and Intercomparisons. *J. Clim.*, **30**, 8179-8205, doi: 10.1175/JCLI-D-16-0836.1. [[Link](#)]
- Huffman, G. J., R. F. Adler, P. Arkin, A. Chang, R. Ferraro, A. Gruber, J. Janowiak, A. McNab, B. Rudolf, and U. Schneider, 1997: The Global Precipitation Climatology Project (GPCP) Combined Precipitation Dataset. *Bull. Amer. Meteorol. Soc.*, **78**, 5-20, doi: 10.1175/1520-0477(1997)078<0005:TGPCPG>2.0.CO;2. [[Link](#)]
- Hung, C. and H.-H. Hsu, 2008: The First Transition of the Asian Summer Monsoon, Intraseasonal Oscillation, and Taiwan Mei-yu. *J. Clim.*, **21**, 1552-1568, doi: 10.1175/2007jcli1457.1. [[Link](#)]
- Hung, C.-S. and C.-H. Sui, 2018: A Diagnostic Study of the Evolution of the MJO from Indian Ocean to Maritime Continent: Wave Dynamics versus Advective Moistening Processes. *J. Clim.*, **31**, 4095-4115, doi: 10.1175/jcli-d-17-0139.1. [[Link](#)]
- Jiang, X., T. Li, and B. Wang, 2004: Structures and mechanisms of the northward propagating boreal summer intraseasonal oscillation. *J. Clim.*, **17**, 1022-1039, doi: 10.1175/1520-0442(2004)017<1022:samotn>2.0.co;2. [[Link](#)]
- Kajikawa, Y. and B. Wang, 2012: Interdecadal change of the South China Sea summer monsoon onset. *J. Clim.*, **25**, 3207-3218, doi: 10.1175/jcli-d-11-00207.1. [[Link](#)]
- Kajikawa, Y. and T. Yasunari, 2005: Interannual variability of the 10-25- and 30-60-day variation over the South China Sea during boreal summer. *Geophys. Res. Lett.*, **32**, L04710, doi: 10.1029/2004GL021836. [[Link](#)]
- Kemball-Cook, S. and B. Wang, 2001: Equatorial waves and air-sea interaction in the boreal summer intraseasonal oscillation. *J. Clim.*, **14**, 2923-2942, doi: 10.1175/1520-0442(2001)014<2923:ewaasi>2.0.co;2. [[Link](#)]
- Lee, H.-T. and NOAA CDR Program, 2011: NOAA Climate Data Record (CDR) of Daily Outgoing Longwave Radiation (OLR), Version 1.2, NOAA National Climatic Data Center, doi: 10.7289/V5SJ1HH2. [[Link](#)]
- Liebmann, B. and C. A. Smith, 1996: Description of a Complete (Interpolated) Outgoing Longwave Radiation Dataset. *Bull. Amer. Meteorol. Soc.*, **77**, 1275-1277.
- Lin, P.-H., Y.-J. Yang, C.-H. Liu, S.-P. Hsu, J.-H. Yang, C.-H. Wu, C.-K. Yu, S. Jan, and C.-H. Sui, 2016: Interaction of Convection over The Maritime Continent - SCS with Large-Scale Flow: 2016 Winter Monsoon Pre-experiment. *Atmos. Sci.*, **44**, 329-352, doi: 10.3966/025400022016124404003. (in Chinese) [[Link](#)]
- Liu, B. and C. Zhu, 2019: Extremely late onset of the 2018 South China Sea summer monsoon following a La Niña event: Effects of triple SST anomaly mode in the North Atlantic and a weaker Mongolian cyclone. *Geophys. Res. Lett.*, **46**, 2956-2963, doi: 10.1029/2018GL081718. [[Link](#)]
- Luo, M., Y. Leung, H.-F. Graf, M. Herzog, and W. Zhang, 2016: Interannual variability of the onset of the South China Sea summer monsoon. *Int. J. Climatol.*, **36**, 550-562, doi: 10.1002/joc.4364. [[Link](#)]
- Madden, R. A. and P. R. Julian, 1971: Detection of a 40-50 day oscillation in the zonal wind in the tropical Pacific. *J. Atmos. Sci.*, **28**, 702-708, doi: 10.1175/1520-0469(1971)028<0702:doadoi>2.0.co;2. [[Link](#)]
- Mao, J., J. C. L. Chan, and G. Wu, 2004: Relationship between the onset of the South China Sea summer monsoon and the structure of the Asian subtropical anticyclone. *J. Meteorol. Soc. Jpn.*, **82**, 845-859, doi: 10.2151/jmsj.2004.845. [[Link](#)]
- Sui, C.-H., P.-H. Lin, W.-T. Chen, S. Jan, C.-Y. Liu, Y.-J. Yang, C.-H. Liu, J.-M. Chen, M.-J. Yang, J.-S. Hong, L.-H. Hsu, and L.-S. Tseng, 2020: The South China Sea Two Islands Monsoon Experiment for studying convection and subseasonal to seasonal variability. *Terr. Atmos. Ocean. Sci.*, **31**, 103-129, doi: 10.3319/TAO.2019.11.29.02. [[Link](#)]
- Tong, H. W., J. C. L. Chan, and W. Zhou, 2009: The role of MJO and mid-latitude fronts in the South China Sea summer monsoon onset. *Clim. Dyn.*, **33**, 827-841, doi: 10.1007/s00382-008-0490-7. [[Link](#)]
- Tsai, W. Y.-H., M.-M. Lu, C.-H. Sui, and P.-H. Lin, 2020: MJO and CCEW modulation on South China Sea and Maritime Continent boreal winter subseasonal peak precipitation. *Terr. Atmos. Ocean. Sci.*, **31**, 177-195, doi: 10.3319/TAO.2019.10.28.01. [[Link](#)]
- Tseng, Y.-H., R. Ding, and X. Huang, 2017a: The warm blob in the northeast Pacific—the bridge leading to the 2015/16 El Niño. *Environ. Res. Lett.*, **12**, 054019, doi: 10.1088/1748-9326/aa67c3. [[Link](#)]
- Tseng, Y.-H., Z.-Z. Hu, R. Ding, and H. Chen, 2017b: An ENSO prediction approach based on ocean conditions and ocean-atmosphere coupling. *Clim. Dyn.*, **48**, 2025-2044, doi: 10.1007/s00382-016-3188-2. [[Link](#)]
- Vimont, D. J., J. M. Wallace, and D. S. Battisti, 2003: The seasonal footprinting mechanism in the Pacific: Implications for ENSO. *J. Clim.*, **16**, 2668-2675, doi: 10.1175/1520-0442(2003)016<2668:tsfmit>2.0.co;2. [[Link](#)]
- Wang, B., R. Wu, and X. Fu, 2000: Pacific-East Asian teleconnection: How does ENSO affect East

- Asian climate? *J. Clim.*, **13**, 1517-1536, doi: 10.1175/1520-0442(2000)013<1517:peathd>2.0.co;2. [[Link](#)]
- Wang, B., R. Wu, and T. Li, 2003: Atmosphere-warm ocean interaction and its impacts on Asian-Australian monsoon variation. *J. Clim.*, **16**, 1195-1211, doi: 10.1175/1520-0442(2003)16<1195:aoiaii>2.0.co;2. [[Link](#)]
- Wang, B., H. Lin, Y. Zhang, and M.-M. Lu, 2004: Definition of South China Sea monsoon onset and commencement of the East Asia summer monsoon. *J. Clim.*, **17**, 699-710, doi: 10.1175/2932.1. [[Link](#)]
- Wang, B., F. Huang, Z. Wu, J. Yang, X. Fu, and K. Kikuchi, 2009: Multi-scale climate variability of the South China Sea monsoon: A review. *Dyn. Atmos. Oceans*, **47**, 15-37, doi: 10.1016/j.dynatmoce.2008.09.004. [[Link](#)]
- Wang, H., F. Liu, B. Wang, and T. Li, 2018: Effects of intraseasonal oscillation on South China Sea summer monsoon onset. *Clim. Dyn.*, **51**, 2543-2558, doi: 10.1007/s00382-017-4027-9. [[Link](#)]
- Weng, S.-P. and J.-Y. Yu, 2010: A CGCM study on the northward propagation of tropical intraseasonal oscillation over the Asian summer monsoon regions. *Terr. Atmos. Ocean. Sci.*, **21**, 299-312, doi: 10.3319/TAO.2009.02.18.01(A). [[Link](#)]
- Wheeler, M. C. and H. H. Hendon, 2004: An All-Season Real-Time Multivariate MJO Index: Development of an Index for Monitoring and Prediction. *Mon. Weather Rev.*, **132**, 1917-1932, doi: 10.1175/1520-0493(2004)132<1917:aarmmi>2.0.co;2. [[Link](#)]
- Wheeler, M. C. and G. N. Kiladis, 1999: Convectively Coupled Equatorial Waves: Analysis of Clouds and Temperature in the Wavenumber-Frequency Domain. *J. Atmos. Sci.*, **56**, 374-399, doi: 10.1175/1520-0469(1999)056<0374:ccewao>2.0.co;2. [[Link](#)]
- WMO, 2017: WMO Guidelines on the Calculation of Climate Normals, WMO-No. 1203, World Meteorological Organization (WMO), Switzerland, 18 pp.
- Zhou, W. and J. C. L. Chan, 2005: Intraseasonal oscillations and the South China Sea summer monsoon onset. *Int. J. Climatol.*, **25**, 1585-1609, doi: 10.1002/joc.1209. [[Link](#)]
- Zhou, W. and J. C. L. Chan, 2007: ENSO and the South China Sea summer monsoon onset. *Int. J. Climatol.*, **27**, 157-167, doi: 10.1002/joc.1380. [[Link](#)]